Internet Electronic Journal of Molecular Design **2004**, *3*, 651–661 ISSN 1538–6414
BioChem Press http://www.biochempress.com

Inter*net* Electronic Journal of Molecular Design

October 2004, Volume 3, Number 10, Pages 651–661

Editor: Ovidiu Ivanciuc

Proceedings of the Internet Electronic Conference of Molecular Design, IECMD 2003
November 23 – December 6, 2003
Part 5

Calculations of Electronic Absorption Spectra and Third–order Polarizabilities of Finite Open Single–wall Carbon Nanotubes of (4,2) with Different Lengths

Wen–Dan Cheng, Dong–Sheng Wu, Xiao–Dong Li, You–Zhao Lan, Ya–Jing Gong, Da–Gui Chen, and Yong–Chun Zhang

Fujian Institute of Research on the Structure of Matter, the Graduate School of the Chinese Academy of Sciences, Laboratory of Materials Chemistry and Physics, Fuzhou, Fujian 350002, People's Republic of China

Received: November 16, 2003; Revised: March 29, 2004; Accepted: May 27, 2004; Published: October 31, 2004

Citation of the article:
W.–D. Cheng, D.–S. Wu, X.–D. Li, Y–Z. Lan, H. Zhang, Y.–J. Gong, D.–G. Chen, and Y.–C. Zhang, Calculations of Electronic Absorption Spectra and Third–order Polarizabilities of Finite Open Single–wall Carbon Nanotubes of (4,2) with Different Lengths, *Internet Electron. J. Mol. Des.* **2004**, *3*, 651–661, http://www.biochempress.com.

Inter*net* Electronic Journal of Molecular Design

BioChem Press
http://www.biochempress.com

Calculations of Electronic Absorption Spectra and Third–order Polarizabilities of Finite Open Single–wall Carbon Nanotubes of (4,2) with Different Lengths[#]

Wen–Dan Cheng,* Dong–Sheng Wu, Xiao–Dong Li, You–Zhao Lan, Ya–Jing Gong, Da–Gui Chen, and Yong–Chun Zhang

Fujian Institute of Research on the Structure of Matter, the Graduate School of the Chinese Academy of Sciences, Laboratory of Materials Chemistry and Physics, Fuzhou, Fujian 350002, People's Republic of China

Received: November 16, 2003; Revised: March 29, 2004; Accepted: May 27, 2004; Published: October 31, 2004

Internet Electron. J. Mol. Des. **2004**, *3* (10), 651–661

Abstract

Motivation. The subjects of electronic absorption and dynamic third–order polarizability spectra of (4,2) carbon nanotubes are studied when the 1D system is made small and converged to tube length of about one nm size. Also the main contributions to optical nonlinearities of the studied system are explored.

Method. B3LYP formalism is carried out for the geometry optimization and time–dependent B3LYP is used to calculate electronic absorption spectra. With the combination of SOS method, the third–order polarizabilities are calculated.

Results. There is a larger gap, blue shift of absorption spectra, smaller third–order polarizabilities in tube axial direction, and smaller anisotropy of polarizability spectra in a shorter finite open (4,2) tubes. Electron transitions from the π bonding to π antibonding orbitals make a significant contribution to the low energy absorption spectrum and third–order polarizability for the (4,2) tubes.

Conclusions. The largest third–order polarizability is in the direction of the polarized and basic light along with the tube axis, and these polarizabilities originate from the one–photon allowed excitation states.

Keywords. Carbon nanotube; density functional theory; sum–over–states; third–order polarizability.

Abbreviations and notations

1D, one–dimensional	DFT, density functional theory
DFWM, degenerate four–wave mixing	EFISHG, electric–field–induced second–harmonic generation
SOS, Sum–over–states	
THG, third–harmonic generation	SWCNT, single–wall carbon nanotube

1 INTRODUCTION

Carbon nanotubes have been the focus of intense interest worldwide since its discovery in 1991. As a simple one–dimensional (1D) nanoscaled structure, single–walled carbon nanotubes (SWCNs)

[#] Presented in part at the Internet Electronic Conference of Molecular Design, IECMD 2003.

* Correspondence author; phone: 86–591–371–3068; fax: 86–591–371–3068; E–mail: cwd@ms.fjirsm.ac.cn.

have been the subject of theoretical and experimental efforts because of their unique properties and potential applications [1–6]. Conceptually, as the length of a SWNT is reduced, it ultimately will reach the limit of a fullerene molecular cluster, a 0D object. In this regard, studies of finite size SWNTs offer a unique opportunity to probe the connection between and evolution of electronic structure in periodic molecular systems. Investigations of finite–sized effects in SWNTs are also important to the future utilization of nanotubes in device applications. Transport experiments on metallic SWNTs have shown that μm long tubes behave as Coulomb islands in single electron transistors [7–8]. The electronic properties of a nanotube with about 5 nm in length and the transition behavior of a nanotube of about 3 nm in length from 1D bulk were studied by Lieber's group [6]. Moreover, the nonlinear optical properties of carbon nanotubes have been of considerable interest, not only because the nonlinear spectrum gives information on their electronic structure, but also because the nonlinear materials can be applied to optical devices [1,5,9]. The carbon nanotubes used in nonlinear optical devices have the promising features at frequencies greater than infrared frequencies of the lattice vibration, and the main contributions to optical nonlinearities originate from the one dimension motion of delocalized π–electrons at a fixed lattice ion configuration. Up today, most of investigators have only focused on SWNTs that have always retained characteristic features of a periodic 1D system. In this study, we will touch on the subjects of electronic absorption and dynamic third–order polarizability spectra when this 1D system is made small and converged to tube length of about one nm size.

2 COMPUTATIONAL PROCEDURES

The geometrical optimizations of the finite open SWCNs (4,2)/56 and (4,2)/72 are carried out at the B3LYP/3–21G level using the DFT method [10] of the GAUSSIAN 98 program [11]. Initial geometries of the tube (4, 2) can be constructed by cut strips and rolled up from an infinite graphite sheet, respectively. The tubes of (4,2)/56 and (4,2)/72 can be specified by the same chiral vectors $\mathbf{C}_h = n\mathbf{a}_1 + m\mathbf{a}_2$ and different translation vectors of **T**, where $\mathbf{a}_1$ and $\mathbf{a}_2$ are graphite primitive lattice vectors with $|\mathbf{a}_1| = |\mathbf{a}_2| = a = (\text{C–C})(3^{1/2})$ and $n = 4$ and $m = 2$, C–C =1.42 Å. The **T** is along the tube axis and orthogonal to $\mathbf{C}_h$, and its magnitude represents the length of the unit cell of the (4,2) tube. Here, the T is about 10 Å for the (4,2)/56 and 14 Å for the (4,2)/72. The tube diameter and chirality are uniquely characterized by [12–14] $d = a(n^2+m^2+nm)^{1/2}/\pi$ and $\cos\theta = (n+m/2)/(n^2+m^2+nm)^{1/2}$, respectively. During the optimized processes, a convergent value of RMS (root–mean–square) density matrix and the critical values of force and displacement are set by default of GAUSSIAN 98 program [11] The obtained values that are less than these criterion are omitted during the calculations. Accordingly, after the convergences of the maximum force, RMS force, maximum displacement, and RMS displacement are reached, the zero of the first derivatives and the positive of the second derivatives are obtained on a potential energy surface for these (4,2) tubes. Hence, a

stationary point of minimum on energy surfaces corresponds to equilibrium geometry of these tubes.

After the optimized geometries of the tubes of (4,2)/56 and (4,2)/72 are obtained, we employ the time–dependent density functional theory [15–16] at the B3LYP/3–21G level (TDB3LYP/3–21G) and run in program of GAUSSIAN98 in the calculations of the transition moments and excited state energies. In the TDB3LYP calculations the core electrons were frozen and inner–shells were excluded from the correlation calculations. The wavefunctions and energy eigenvalues of the excited states were determined by solving time–dependent Kohn–Sham equation [15]. The SCF convergence criterion of the RMS density matrix and the maximum density matrix is set at 10^{-8} and 10^{-6}, respectively in the excited state calculations. The iterations of excited states are continued until the changes on energies of states are no more than 10^{-7} au between the iterations, and the convergence has been obtained in the all calculations of excited states. Here noted that the 3–21G basis sets are selected in the B3LYP calculations because we only consider systematic comparisons and variation trends between the calculated results of (4,2) tubes of different lengths.

The tensor components of the frequency–dependent and nonresonant third–order polarizability γ of the tubes of (4,2)/56 and (4,2)/72 are calculated by the conventional sum–over–states (SOS) method [17–18]:

$$\begin{aligned}\gamma_{abcd}(-\omega_p;\omega_1,\omega_2,\omega_3) &= (2\pi/h)^3 K(-\omega_p;\omega_1,\omega_2,\omega_3)e^4\{\Sigma_P \\ &[\Sigma'_{i,j,k}(<o|r_a|k><k|r_b^*|j><j|r_c^*|i><i|r_d|o>)/((\omega_{ko}-\omega_p)(\omega_{jo}-\omega_1-\omega_2)(\omega_{io}-\omega_1))] \\ &-\Sigma_P[\Sigma'_{j,k}(<o|r_a|j><j|r_b|o><o|r_c|k><k|r_d|o>)/((\omega_{jo}-\omega_p)(\omega_{jo}-\omega_1)(\omega_{ko}+\omega_2))]\}\end{aligned} \quad (1)$$

Hereafter γ(3ω), γ(2ω), and γ(ω) symbolizes the third–order polarizability of third–harmonic generation (THG) of γ(–3ω;ω,ω,ω), electric–field—induced second–harmonic generation (EFISHG) of γ(–2ω;ω,ω,0) and degenerate four–wave mixing (DFWM) of γ(–ω;ω,ω,–ω), individually. The prefactor $K(-\omega_p;\omega_1,\omega_2,\omega_3)$ must be taken as the same value for the THG, EFISHG, and DFWM at the static case of an input photon energy of zero, and it is the relative magnitudes of the ground state nonlinear polarizabilities for each optical process at nonzero frequency. [18]. In the following calculations, we use the same prefactor K in order to make the remark to justify plotting curves for the three types of nonlinear polarizability against common axes. Here, it is noted that the Eq. (1) does not include linewidth (or damping factor iΓ) terms in the frequency denominators because the ω_1, ω_2, and ω_3 (as well as their arbitrary linear combinations) can be chosen to be away from a resonant frequency in practical calculations. In this way, although the damping factors are not included in this equation the resonant divergences could be avoided in our calculations. In Eq. (1), the energy differences of $\hbar\omega$, transition moments and dipole moments can be obtained from the calculated results at the TDB3LYP/3–21G level.

3 RESULTS AND DISCUSSION

3.1 Configuration and Natural Orbital Populations

Figure 1 shows the optimized geometrical structures of finite open SWCNs (4,2) with different tube axial lengths. They consist of 56 and 72 carbon atoms, hereafter written as (4,2)/56 and (4,2)/72, respectively. The tube diameters of the (4,2)/56 and (4,2)/72 are both about 4.3 Å, and the average tube axial length is about 10.08 and 13.24 Å, respectively. The C–C length range is between 1.397 and 1.487 Å and well falls between single (1.54 Å) and double (1.34 Å) bonds except the C–C bonds of tube ends. The dangling bonds remain unsaturated and the tube has six edge atoms at each end. The unpaired electrons at the edge of the nanotubes attempt to establish a double bond and even triple bond with their neighbors. There are two pairs of C–C bonds being 1.250 Å at each end of open tube, and the C–C lengths have triplet bond character (1.20 Å). The bond lengths of the optimized structures at the tube ends are substantially different from those of an ideal rolling of a graphene sheet.

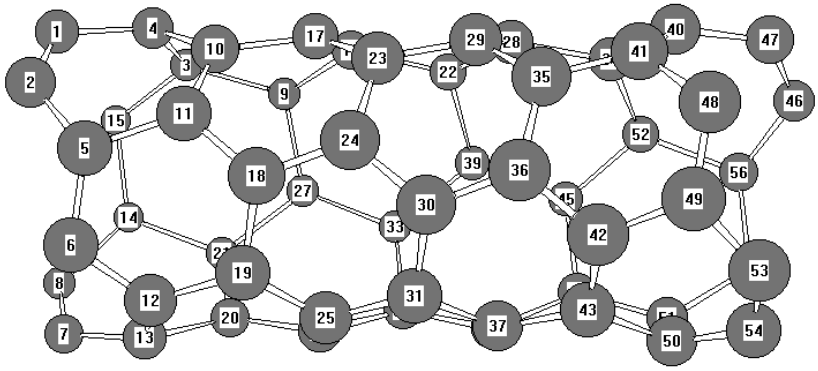

(4,2)/56

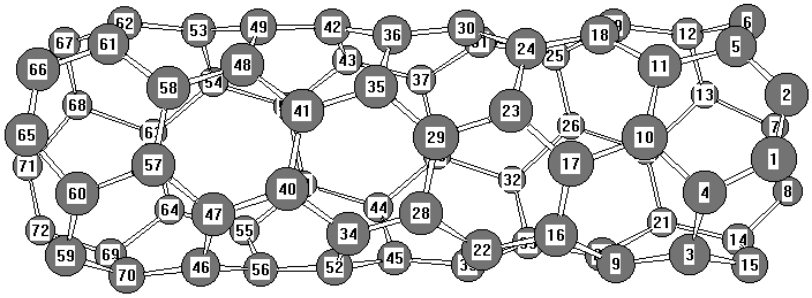

(4,2)/72

Figure 1. The optimized geometrical structures of finite open SWCNs (4,2).

The natural bond orbital (NBO) analysis is obtained from the molecular orbital calculations using the B3LYP/3–21G model. The nonbonding and triplet bonding orbitals appear at each end of open tube and the occupancies and energies of selected NBOs concerning about the tube end atoms

are listed in Table 1 (here only one pair of C–C atoms is listed). For example, the triplet–bonding of C_1–C_2 has occupancies of 5.602 e, and the nonbonding occupancy of C_6, C_{12}, C_{15} is 1.503, 1.003, and 1.503 e, individually, for the (4,2)/56 carbon tube.

Table 1. The natural bond orbital analysis for the end atoms of carbon tubes based on the B3LYP/3–21G level

(4,2)/56					
		bonding		antibonding	
bond	length (Å)	occupancy (e)	energy (a.u.)	occupancy (e)	energy (a.u.)
C_1–C_2 (1)	1.250	1.98774	–0.85817	0.01529	0.75003
(2)		1.93328	–0.31979	0.09426	0.04330
(3)		1.68086	–0.31962	0.20409	0.05459
lone pair C_6		1.50300	–0.26075		
C_{12}		1.00345	–0.17163		
(4,2)/72					
C_1–C_2 (1)	1.250	1.98800	–0.86342	0.01424	0.74347
(2)		1.93044	–0.32959	0.08097	0.04492
(3)		1.66555	–0.32323	0.20932	0.04863
lone pair C_6		1.55585	–0.26257		
C_{12}		1.07895	–0.17115		

3.2 Electronic Absorption Spectrum

The calculated electronic absorption spectra of the finite open SWCNs (4,2) with the different tube axial lengths are shown in Figure 2. The shapes and sites of spectra are expected with a broad band at the low energy absorption zone and sharp peaks at the higher energy zone. The absorption bands of S_i (i = a, b, c, d) mostly originate from an axial allowed, and S_e mostly originate from an radical allowed electron transition from the ground state to excited states. These evidences are given by the transition moments in the axial (x) and radial (y,z) directions, as listed in Table 2.

Table 2. Calculated transition energies and moments based on TDB3LYP/3–21G level for finite open SWCNs (4,2)

(4,2)/56					(4,2)/72				
peak	energy	moments (au)			peak	energy	moments (au)		
site	(eV)	x	y	z	site	(eV)	x	y	z
a	0.7035	1.3504	0.0000	–0.0001	a	0.4568	–1.0276	0.0917	0.0307
b	1.6100	–0.5953	–0.0007	–0.0005	b	1.1507	–0.4516	–0.0631	–0.0468
c	1.9043	0.5690	0.0000	–0.0001	c	1.6739	0.0639	–0.0592	–0.2531
d	2.1643	0.3980	0.0000	0.0002	d	1.8253	0.2277	0.0599	–0.0757
e	2.1718	0.0000	0.6102	0.0000	e	1.9840	0.1625	–0.1316	0.2717

The first absorption peak S_a localized at 1762 nm is contribution from the ground singlet state to excited singlet state S_3 and the transition moment is 1.350, and 0.000 a.u at the *x*, and *y*, *z* directions, respectively, for the (4,2)/56 carbon tube. The transition moment from the ground state to excited state S_{25} contributing to absorption peak S_e is 0.000, 0.610 and 0.000 a.u. at the x, and y, z directions in turn for the (4,2)/56 tube. An analysis in terms of the NBO calculations, it is found that the absorption peak of S_a and S_e is separately mainly contributions from the electron transition from the lone pair (nonbonding) π occupancies to π* and to σ* antibonding of C–C triplet bond (n_π–$\pi^*_{p–p}$ and n_π–$\sigma^*_{p–p}$ electron transition, as listed the occupancies of antibondings of C_1–C_2 (2), (3), and (1)

and lone pair C at Table 1). Comparing the absorption spectra between the two tubes, we find that the spectrum of (4,2)/72 tube with a larger axial length (about 13 Å) gives a red shift of the first absorption peak with respect to the (4,2)/56 tube.

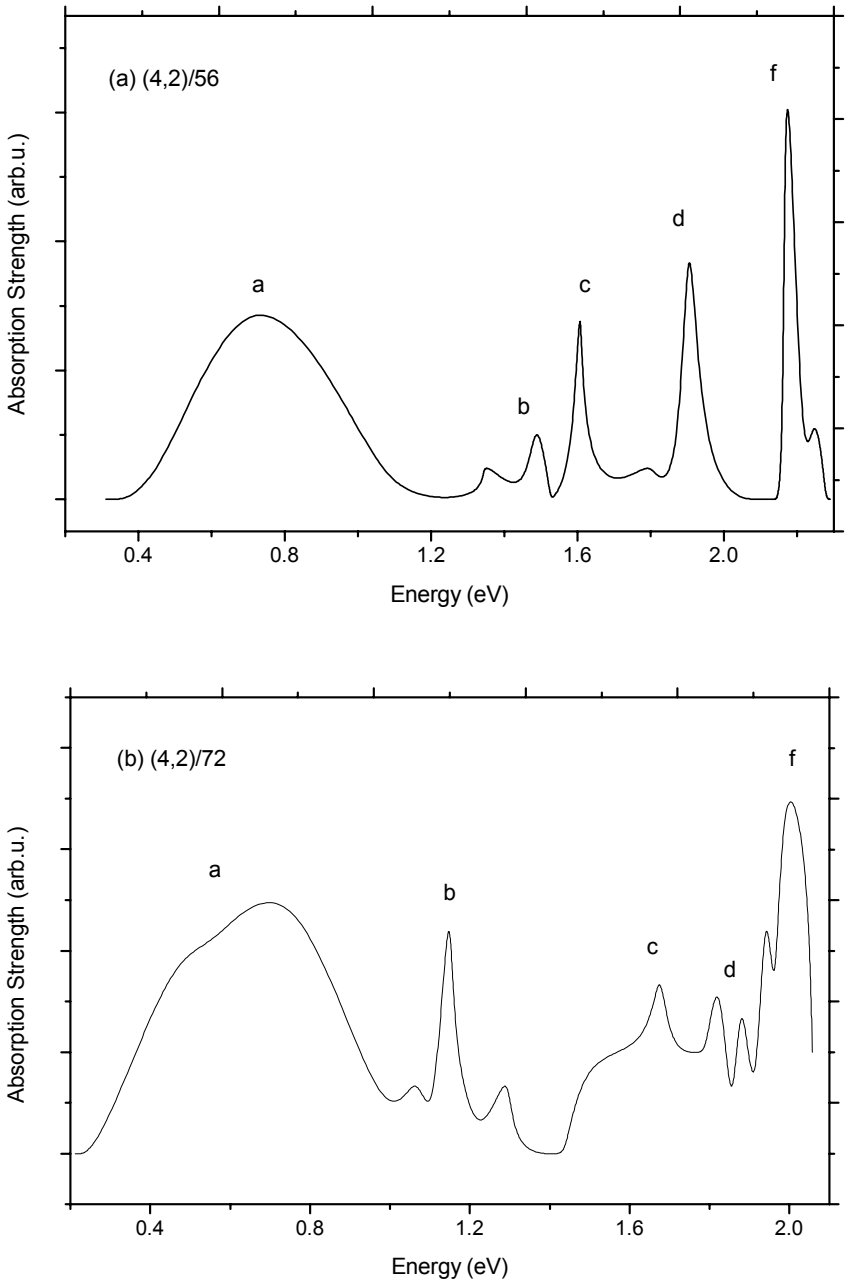

Figure 2. The calculated electronic absorption spectra of single–walled tubes (4,2) based on TDB3LYP/3–21G level.

3.3 Third–order nonlinear optical properties

Before attempting to compute the variation of the third–order polarizability *vs*. wavelength, it is necessary to investigate the behavior of the convergence in the summation of excited states and to

determine whether the results calculated from the TDB3LYP method are reliable for the finite open SWCNs (4,2)/56 and (4,2)/72. Figure 3 shows the plots of the calculated third–order polarizabilities, γ_a (γ_{xxxx}), for which the polarizability is along with the axial direction of tubes, *vs*. the number of states at static case. It is found that the calculated value of γ_a including 14 and 6 excited states is about 95% and 93% of γ_a value including 50 states, respectively, for the tubes of (4,2)/56 and (4,2)/72. These facts show a reasonable approximation truncating the infinite SOS expansion to a finite one over about 50 states in our calculations of γ.

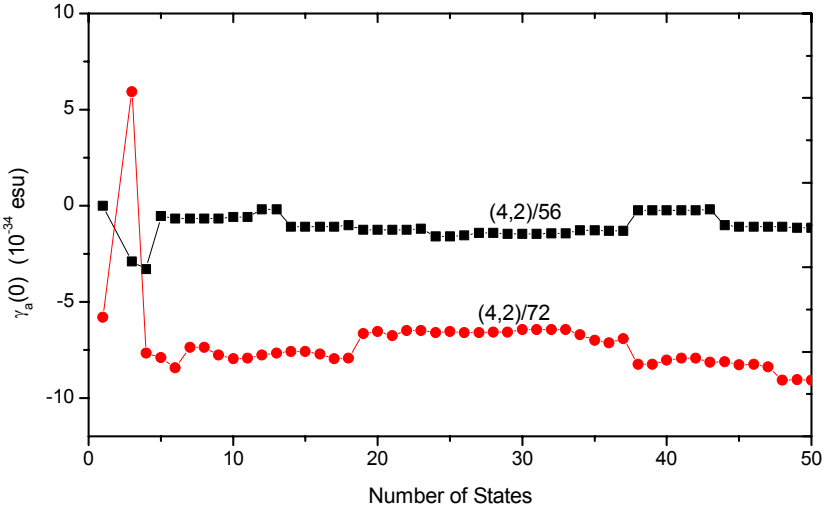

Figure 3. The calculated state–dependent third–order polarizabilities of tubes (4,2)/56 and (4,2)/72 at the SOS//TDB3LYP/3–21G level at input photon energy of zero.

Table 3. The calculated static polarizabilities of γ (10^{-36} esu) based on SOS//TDB3LYP/3–21G level

Tube	γ_{xxxx}	γ_{yyyy}	γ_{zzzz}	$\gamma_{xxyy}(=\gamma_{yyxx})$	$\gamma_{xxzz}(=\gamma_{zzxx})$	$\langle\gamma\rangle$*
(4,2)/56	–114.50	2.29	9.40	38.90	101.74	36.62
(4,2)/72	–907.06	54.12	3.85	421.81	43.74	17.90

$\langle\gamma\rangle = 1/5(\gamma_{xxxx} + \gamma_{yyyy} + \gamma_{zzzz} + \gamma_{xxyy} + \gamma_{xxzz} + \gamma_{yyxx} + \gamma_{yyzz} + \gamma_{zzxx} + \gamma_{zzyy})$

Figure 4 depict the calculated dynamic third–order polarizabilities of γ_a having different optical physical processes from frequency 0.0 to 1.20 eV/ħ at the ground state. It is shown that the enhancement oscillating bands appear at larger than 0.35 eV and 0.25 eV for the finite open SWCNs (4,2)/56 and (4,2)/72. For static case where the input photon energy is zero, the γ_a values of all three processes of the THG, EFISHG, and DFWM have the same values of -1.145×10^{-34}, and -9.071×10^{-34} esu for the tubes (4,2)/56 and (4,2)/72, respectively. Furthermore, in order to describe the anisotropy of nonlinear polarizabilities of the tubes (4,2)/56 and (4,2)/72, Table 3 lists the calculated third–order polarizabilities at the radial and axial directions of the tubes in the static case.

It is shown that the absolute value of largest third–order polarizability is in the direction of the polarized and basic light along with the tube axis. Comparing the third–order polarizabilities of the (4,2)/56 tube and those of the (4,2)/72 tube, we found that the anisotropy of polarizabilities is larger for the (4,2)/72 than (4,2)/56 tube, and there is a larger third–order polarizability in the axial direction while there is a larger axial length in the finite open SWCNs of (4,2).

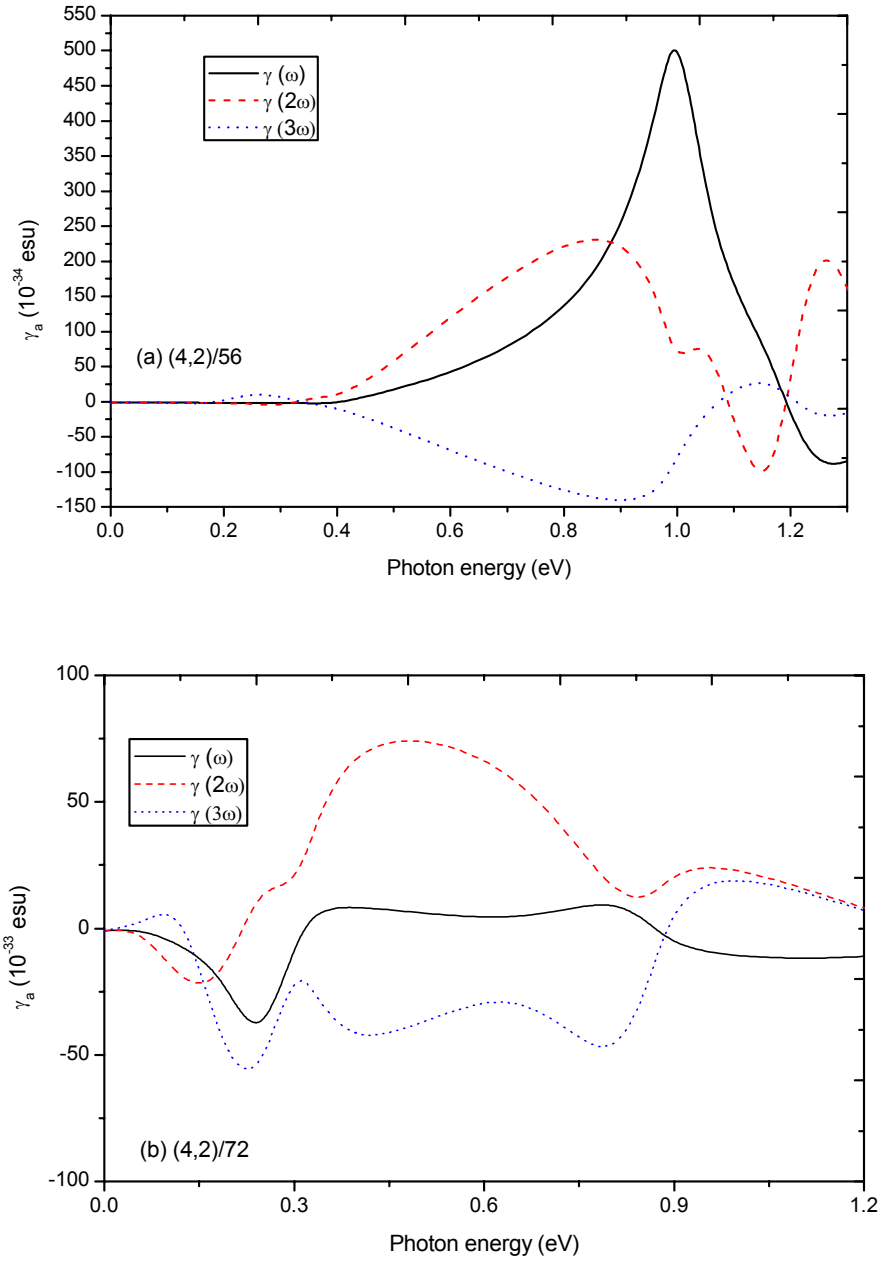

Figure 4. The calculated frequency–dependent third–order polarizabilities of different optical processes at SOS//TDB3LYP/3–21G level for (4,2) tube.

Now, we are going to discuss the electronic origin of third–order polarizabilities of the tubes of (4,2)/56 and (4,2)/72. In the SOS formula of Eq. (1), we can see the value of third–order polarizability comes from the summations of type–I (second term of right in the equation) and type–II terms (first term of right in the equation). These two terms are the competing third–order virtual excitation processes, and the electron transitions between two states in each term are fit for the dipole selection rules. The type–I processes are of the form $S_g \rightarrow S_m \rightarrow S_g \rightarrow S_m \rightarrow S_g$, where S_g is the ground state and S_m is a one–photon allowed excited state. The intermediate state is S_g itself, and this process makes a negative contribution to γ at a low frequency region. For example, the calculated $(\gamma_a(0))_I$ is -5.255×10^{-34}, and -29.137×10^{-34} esu at static case for the tubes of (4,2)/56 and (4,2)/72, respectively. For the type–II processes, $S_g \rightarrow S_m \rightarrow S_n \rightarrow S_m \rightarrow S_g$, the intermediate state S_n is a two–photon allowed excited state. The calculated $(\gamma_a(0))_{II}$ is 4.110×10^{-34}, and 20.066×10^{-34} esu at static case for the tubes of (4,2)/56 and (4,2)/72. By the comparisons between the two processes, we find that the type–I process makes a larger, negative contribution to γ_a, and therefore determines the overall sign of γ_a to be negative. That is, the one–photon excitation processes greatly win a triumph over the two–photon excitation processes at low frequent zone. As the above–mentioned descriptions, the type–I processes are the one–photon allowed virtual excited processes.

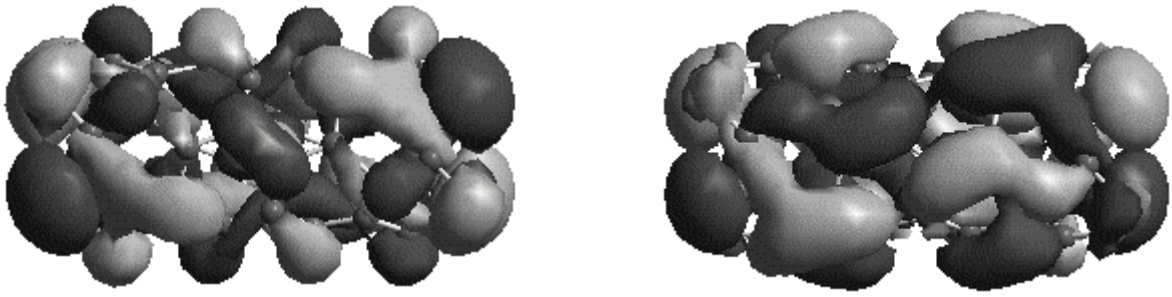

HOMO–1 LUMO

Figure 5. The molecular orbitals contributing to the configuration of $\psi_{167->169}$.

Accordingly, we can say that the one–photon allowed excited singlet states make major contributions to the third–order nonlinear polarizabilities of the ground state of the tubes (4,2)/56 and (4,2)/72, respectively. Furthermore, we will understand what are the constructions of one–photon states mostly contributing to third–order polarizabilities. For the tube (4,2)/56, the calculated $\gamma_a(0)_I$ value using only state 3 is *ca*. 55% of the $\gamma_a(0)_I$ (reached convergence) calculated from summation over about 50 states at static case.

The state 3 has the greatest contribution from the configuration $\psi_{167->169}$. This configuration is constructed by one electron from double occupied molecular orbital 167 (HOMO–1) to unoccupied molecular orbital 169 (LUMO). The molecular orbitals contributing to the configuration of $\psi_{167->169}$ are plotted in Figure 5. They are mostly formed from π–orbitals, and the atoms localized at tube ends have larger charges distributions. With the same analytic process, we also find that the one–photon state mainly contributing to third–order polarizabilities are most contributions from the π–electron occupied and unoccupied orbitals.

4 CONCLUSIONS

The geometrical structures of finite open SWCNs (4,2) with different axial lengths have been optimized based on the B3LYP/3–21G level, and the structures show that the bond lengths and angles of the tubes, in particularly, at the tube ends, are substantially different from those of an ideal rolling of a graphene sheet. The calculated electronic absorption spectra based on the TDB3LYP/3–21G level indicates that the shapes of spectra are broad at the low energy absorption zone, which is axial allowed electronic transitions, and sharp peaks at the higher energy zone, which is radical allowed transition.

The dynamic third–order optical polarizabilities in the THG, EFISHG, and DFWM optical processes have been obtained by the SOS combined with the TDB3LYP methods for the optimized configurations of the (4,2) tubes. The obtained results show that the largest third–order polarizability is in the direction of the polarized and basic light along with the tube axis, and these polarizabilities originate from the one–photon allowed excitation states.

Acknowledgment

This investigation was supported by the National Science Foundation of China (No. 90201015), the Science Foundation of the Fujian Province (No. E0210028 and No. 2002F010), and the Foundation of State Key Laborator of Structural Chemistry (No. 030060).

5 REFERENCES

[1] H. Han, S. Vijayalakshmi, A. Lan, Z. Lqbal, H. Grebel, E. Lalanne and A. M. Johnson, *Appl*. *Phys*. *Lett*. **2003**, *82*, 1458–1460.

[2] W. Liang, G. Chen, Z. Li and Z.–K. Tang, *Appl*. *Phys*. *Lett*. **2002**, *80*, 3415–3417.

[3] H. J. Liu and C. T. Chan, *Phys*. *Rev*. *B* **2002**, *66*, 115416.

[4] M. Machon, S. Reich, C. Thomsen, D. Sanchez–Portal, P. Ordejon, *Phys*. *Rev*. *B* **2002**, *66*, 155410.

[5] S. Wang, W. Huang, H. Yang, Q. Gong, Z. Shi, X. Zhou, D. Qiang, Z. Gu, *Chem*. *Phys*. *Lett*. **2000**, *320*, 411–414.
[6] T. W. Odom, J.–L. Huang, P. Kim, and C. M. Lieber, *J. Phys*. *Chem*. *B* **2002**, *104*, 2794–2809.
[7] M. Bockrath, D. H. Cobden, P. L. McEuen, N. G. Chopra, A. Zettl, A. Thess, R. E. Smalley, *Science* **1997**, *275*, 1922–1925.
[8] S. J. Tans, M. H. Devoret, H. Dai, A. Thess, R. E. Smalley, L. J. Geerligs, C. Dekker, *Nature* **1997**, *386*, 474–477.
[9] C. Stanciu, R. Ehlich, V. Petrov, O. Steinkellner, J. Herrmann, I. V. Hertel, G. Ya. Slepyan, A. A. Khrutchinski, S. A. Maksimenko, F. Rotermund, E. E. B. Campbell, F. Rohmund, *Appl*. *Phys*. *Lett*. **2002**, *81*, 4064–4066.
[10] A. D. Becke, *J. Chem*. *Phys*. **1993**, *98*, 5648–5652.
[11] Gaussian 98 (Revision A.9), M. J. Frisch, G. W. Trucks, H. B. Schlegel, G. E. Scuseria, M. A. Robb, J. R. Cheeseman, V. G. Zakrzewski, J. A. Montgomery, R. E. Stratmann, J. C. Burant, S. Dapprich, J. M. Millam, A. D. Daniels, K. N. Kudin, M. C. Strain, O. Farkas, J. Tomasi, V. Barone, M. Cossi, R. Cammi, B. Mennucci, C. Pomelli, C. Adamo, S. Clifford, J. Ochterski, G. A. Petersson, P. Y. Ayala, Q. Cui, K. Morokuma, D. K. Malick, A. D. Rabuck, K. Raghavachari, J. B. Foresman, J. Cioslowski, J. V. Ortiz, B. B. Stefanov, G. Liu, A. Liashenko, P. Piskorz, I. Komaromi, R. Gomperts, R. L. Martin, D. J. Fox, T. Keith, M. A. Al–Laham, C. Y. Peng, A. Nanayakkara, C. Gonzalez, M. Challacombe, P. M. W. Gill, B. G. Johnson, W. Chen, M. W. Wong, J. L. Andres, M. Head–Gordon, E. S. Replogle and J. A. Pople, Gaussian, Inc., Pittsburgh PA, 1998.
[12] J. W. Ding, X. H. Yan, and J. X. Cao, *Phys*. *Rev*. *B* **2002**, *66*, 073401.
[13] M. S. Dresselhaus, *Nature* **1998**, 391, 19–20; *Science* **2001**, *292*, 650–651.
[14] C. Dekker, *Phys*. *Today* **1999**, *52*, 22–28.
[15] R. Bauernschmitt, R. Ahlrichs, *Chem*. *Phys*. *Lett*. **1996**, *256*, 454–464.
[16] R. E. Stratmann, G. E. Scuseria, M. J. Frisch, *J. Chem Phys*. **1998**, *109*, 8218–8224.
[17] B. J. Orr, J. F. Ward, *Mol*. *Phys*. **1971**, *20*, 513.
[18] B. M. Pierce, *J. Chem*. *Phys*. **1989**, *91*, 791.

Biographies

Wen–Dan Cheng is Professor at Fujian Institute of Research on the Structure of Matter, Chinese Academy of Sciences. After obtaining Master degree from the Department of Chemistry in Xiamen University in 1981, his primary research interests include the structural control and molecular design of optical materials, as well as the linear and nonlinear optical responses at nanosize and extended systems through the theoretical and experimental treatments.